Astron. Astrophys. 322, 846–856 (1997)

ASTRONOMY
AND
ASTROPHYSICS

Origin of pulsar radio emission

I. High frequency data

M. Kramer[1], **K.M. Xilouris**[2], **A. Jessner**[1], **D.R. Lorimer**[1], **R. Wielebinski**[1], **and A.G. Lyne**[3]

[1] Max-Planck-Institut für Radioastronomie, Auf dem Hügel 69, D-53121 Bonn, Germany
[2] National Astronomy and Ionospheric Center, Arecibo Observatory, P.O. Box 995, Arecibo, Puerto Rico 00613
[3] University of Manchester, Nuffield Radio Astronomy Laboratories, Jodrell Bank, Macclesfield, Cheshire, SK11 9DL, UK

Received 20 June 1996 / Accepted 12 December 1996

Abstract. Using the pulse arrival times from pulsar observations made between 1.4 and 32 GHz, we constrain the location and size of the magnetospheric region which is responsible for the observed radio emission. We demonstrate that for long period pulsars the magnetic field maintains its dipolar form throughout the whole emission region. The emission region itself is located very close to the stellar surface and confined to a small slab of a few tens stellar radii in height.

Key words: pulsars: general – pulsars: individual: B0329+54, B0355+54, B0540+32, B1133+16, B1706-16, B1929+10, B2020+28, B2021+51 – radiation mechanisms: miscellaneous

1. Introduction

A long standing question in pulsar astronomy has been the location of the radio emission. Three places have been suggested; near the light cylinder (Smith 1969), perhaps located in regions of closed magnetic field lines (Gold 1968), and the open field line regions (Radhakrishnan & Cooke 1969). Nowadays, it is widely accepted (see e.g. Lyne & Smith 1990) that the radio emission originates from the open field line region well inside the light cylinder, whereas the very high energy emission (optical and above) probably arises in a quite different mechanism, much nearer to the light cylinder.

The concept of a *radius-to-frequency mapping* (RFM) i.e. the model that radio emission of a certain frequency, ν, is radiated at a particular distance, $r_{em}(\nu)$, above the neutron star surface was first thoroughly discussed by Cordes (1978). In fact RFM already exists in several theoretical models. Ruderman & Sutherland (1975), for instance, assumed that the radiation frequency is related to the local plasma frequency. The plasma frequency decreases with distance from the star as the particle density becomes smaller while the plasma flows along the spreading field lines. Therefore, lower frequency radiation is emitted as the plasma frequency decreases away from the star surface. Such a frequency dependence of the emission height can easily explain the observed narrowing of the profile width and component separation with increasing frequency (Sieber et al. 1975).

Such changes in the pulse profile widths are considered to be the best arguments in favour of the existence of a RFM, although they may also be interpreted differently (e.g. by as a dependence on the longitudinal separation to the magnetic axis, see Rickett & Cordes 1981). However, RFM fits in an attractive way to polar cap models where emission comes from the open field line region. Measurements of the profile widths at various frequencies can then be used to deduce the emission heights if dipolar field lines are assumed (Cordes 1978).

In addition to this *geometrical* method in order to place limits on the location of the emission region, *timing* data obtained at several frequencies can be used to look for delays in the expected arrival times of pulses caused by retardation, aberration effects or a possible magnetic sweep-back near the light cylinder. Blaskiewicz et al. (1991, hereafter BCW) used another independent method by deducing absolute emission altitudes from high quality *polarimetry* data. In their relativistic correction to the classical rotating-vector model of Radhakrishnan & Cooke (1969), they predicted a time delay between the centroids of the pulse profile and the corresponding polarisation position angle curve. BCW determined this delay for several profiles and determined emission altitudes for 0.408 GHz and 1.400 GHz emission. The same method was recently applied by Hoensbroech & Xilouris (1997) to data obtained between 1.400 GHz and 10.550 GHz. Both studies found a general good agreement with the results obtained from the geometrical method based on the profile width (cf. also Xilouris et al. 1996).

Interestingly, most of these studies were made at frequencies below 5 GHz, and rather little is known about the validity of a RFM at high frequencies (see Kramer et al. 1994, Xilouris et al. 1996, Hoensbroech & Xilouris 1997). This is of great importance, since emission observed at very high radio frequencies should originate from locations very close to the stellar

Send offprint requests to: M. Kramer (mkramer@mpifr-bonn.mpg.de)

surface, where the assumption of dipolar field lines might not hold true any longer but magnetic multipoles might become important (Wolszczan et al. 1980, BCW). In fact some observers have already claimed the detection of magnetic multipoles based on observations made at about 5 GHz (e.g. Davies et al. 1984, Kuzmin 1986).

The detection of pulsars at the highest radio frequencies ever (Wielebinski et al. 1993, Kramer et al. 1996), raises the question about the origin of the observed radiation. According to the canonical RFM it should be created closer to the neutron star surface than any other radio pulsar emission observed before. Here (paper I) and in a subsequent paper (paper II), we will try to place constraints on the size and location of the emission region by appling timing data obtained at various frequencies. In this paper, we will focus on the high frequency regime, i.e. on profiles observed between 1.4 GHz to 32 GHz with the MPIfR's 100m-radiotelescope in Effelsberg. A combination of the high frequency data with a corresponding low frequency data set observed with the 76m-Lovell telescope in Jodrell Bank will be presented in paper II.

The outline of this paper is as follows. We review in Sect. 2 all the important effects relevant for our analysis of the data. The details of our observations are given in Setc. 3. In Sect. 4 we explain the data analysis and present individual results in the Sect. 5. In Sect. 6 we will discuss the results obtained from the high frequency data set and compare them to previous results before finally conclusions are drawn.

2. Background

In what follows we will assume that RFM exists. In other words, the radiation received at a particular frequency, ν, can be clearly mapped to a certain altitude above the neutron star surface, r_{em}, where the emission takes place. We are interested in the absolute value of the emission altitude as well as its dependence on frequency, generally assumed to be a power law,

$$r_{em} \propto \nu^{-\kappa}. \tag{1}$$

Under this assumption, we might be able to observe a difference in the times-of-arrival (TOAs) of a pulse profile observed at different frequencies. Several contributions to this time difference are possible. Following Phillips (1991b; 1992, hereafter P92), we take four major effects into account.

Retardation: The most obvious contribution is a simple *retardation delay*. Let us consider a pulse emitted at two frequencies ν_1 and ν_2 with $\nu_2 > \nu_1$. If the corresponding radiation is created at radii r_1 and r_2, respectively, then we expect a delay, Δt_{ret} due to the different path lengths as simply given by

$$\Delta t_{ret} = T_{ret}(\nu_2) - T_{ret}(\nu_1) = \frac{r_1 - r_2}{c}. \tag{2}$$

Here we have chosen the sign in the sense that Δt_{ret} is positive if

$$\nu_1 < \nu_2 \qquad \text{and} \qquad r_1 \equiv r_{em}(\nu_1) > r_{em}(\nu_2) \equiv r_2 \tag{3}$$

is fulfilled.

Dispersion: Pulses propagating through the interstellar medium suffer a frequency dependent dispersion delay, so that the difference in the arrival times of pulses observed at two different frequencies, ν_1 and ν_2, is given by

$$\Delta t_{DM} = T_{DM}(\nu_2) - T_{DM}(\nu_1) = \alpha_D^{-1}\ DM\ \left(\nu_2^{-2} - \nu_1^{-2}\right) \tag{4}$$

with DM as the electron column density along the path to the pulsar, which is called *dispersion measure* and usually quoted in units of cm^{-3}pc. The *dispersion constant*, α_D, is defined as $\alpha_D = 2\pi m_e c/e^2$, where m_e and e are the mass and charge of an electron, respectively. Dispersion measures are usually quoted for a value of $\alpha_D = 2.41 \cdot 10^{-16}$ cm^{-3} pc s, rather than for the physical value of $\alpha_D = 2.410332 \cdot 10^{-16}$ cm^{-3}pc s (Manchester & Taylor 1977).

Aberration: The rotation of the neutron star causes a bending of the radiation beam towards the rotational direction (cf. BCW). The corresponding deflection angle Θ_{ab} depends on the emission altitude, r_{em}, and is given (after P92) by

$$\Theta_{ab} = \arctan\left(2\pi \frac{r_{em}\ \sin\alpha}{c\ P}.\right) \tag{5}$$

In this expression, α is the inclination angle between spin and magnetic axis and P the pulse period. An outside observer will, therefore, receive the pulse earlier by a fraction of $\Theta_{ab}/2\pi$ of the pulse period if Θ_{ab} is measured in radians. Translated into time, the difference between the TOAs of signals received at two different frequencies is given by

$$\begin{aligned}\Delta t_{ab} &= T_{ab}(\nu_2) - T_{ab}(\nu_1) \\ &= \frac{P}{2\pi}\left[\Theta_{ab}(\nu_2) - \Theta_{ab}(\nu_1)\right],\end{aligned} \tag{6}$$

where the sign is chosen in the sense of Eq. (3). In the case that the emission region is located well inside the light cylinder, i.e. $r_{1,2} \ll cP/2\pi \equiv R_L$, the relation simplifies to

$$\Delta t_{ab} = \sin\alpha \cdot \left(\frac{r_1 - r_2}{c}\right) = \sin\alpha \cdot \Delta t_{ret} \tag{7}$$

Magnetic field sweep-back: Particles outflowing the open magnetic field lines will cause a toroidal component of the magnetic field near the light cylinder. As a result, the field lines will be swept back, i.e. bend towards a direction opposite to the sense of rotation. Following Shitov (1983) and P92, the sweep-back angle is given by

$$\Theta_{msb} \simeq 1.2\left(\frac{2\pi r_{em}}{cP}\right)^3 \sin^2\alpha \tag{8}$$

which gives rise to a time delay of approximately

$$\begin{aligned}\Delta t_{msb} &= T_{msb}(\nu_2) - T_{msb}(\nu_1) \\ &= 1.2\frac{4\pi^2}{c^3 P^2}\left(r_2^3 - r_1^3\right)\sin^2\alpha.\end{aligned} \tag{9}$$

Adding these major contributions we obtain for the total time difference

$$\begin{aligned}\Delta t_{tot} &= TOA(\nu_2) - TOA(\nu_1) \\ &= \Delta t_{ret} + \Delta t_{DM} + \Delta t_{ab} + \Delta t_{msb}.\end{aligned} \tag{10}$$

Within the canonical model that high frequency emission originates from closer to the neutron star than low frequency emission, i.e. validity of relation Eq.(3), the first and third term are positive while the second and last contribution are negative. In other words, while retardation and aberration effects are delaying the high frequency emission (with respect to low frequency emission), dispersion and magnetic field sweep back act in just the opposite way.

Since previous results indicate that even the low frequency emission takes place well inside the light cylinder (e.g. Cordes 1978, Matese & Whitmire 1980, BCW, P92 or Kijak & Gil 1996), we make use of the simpler expression for the aberration delay and obtain

$$\Delta t_{tot} = \frac{\Delta r_{em}}{c}\left[1+\sin\alpha - 1.2\frac{\sin^2\alpha}{R_L^2}\left(r_1^2+r_1r_2+r_2^2\right)\right] + \Delta t_{DM} \quad (11)$$

where we have introduced

$$\Delta r_{em} \equiv r_1 - r_2 = r_{em}(\nu_1) - r_{em}(\nu_2) \quad (12)$$

and used $R_L = cP/2\pi$ [1]. Knowing the exact dispersion delay, Δt_{DM}, and the magnetic inclination, α, on the right hand side, we can measure the total time delay to determine or constrain Δr_{em}.

3. Observations

For reasons detailed later, most of the analyzed profiles were obtained within a short period of about three weeks in Summer 1994, using the 100m-radiotelescope of the MPIfR. In general, we observed at five different frequencies between 1.4 GHz and 32 GHz presented in Table 1, whereas all but the 1.4 GHz observations were made with receivers installed in the secondary focus of the telescope. The signals were detected across the full bandwidth and digitized by 10-MHz V/f-converters. The data were sampled and folded synchronously with the topocentric pulse period before a sub-integration of about 15s was transferred to disk. Pulse profiles at 2.25 GHz were measured simultaneously with data at 8.5 GHz using a dual frequency system. For this frequency only signals of one circular polarisation were available, while all other profiles represent total power data. A calibration signal of an external noise diode was switchable synchronously to the pulse period and ensured that possible gain differences were removed while creating total power profiles. Further details about the observing system are given by Seiradakis et al. (1995) or Kramer (1995).

For some pulsars, we include profiles obtained at 1.41 GHz, although these profiles were generally observed at a later epoch. Observations at this low frequency also involved an incoherent pulse de-disperser, consisting of four 60×0.667 kHz filterbanks and a digital delay line. Its construction principle causes a small additional time delay of the signals due to the rise time of the built-in narrow filters and the delay line used for the online de-dispersing. Although these offsets in the times-of-arrival (TOAs) can be corrected for, we use such filterbank data only in those cases where the precision of the determined TOA is not affected by these offsets anyway, or where additional physical insight is gained. The profiles at all other frequencies were measured by detecting narrow or broad band signals directly (see Table 1), so that significant instrumental delays can be excluded. If we include profiles obtained at epochs different from those given in the Table 1, it is explicitly stated during the discussion of the results.

[1] Applying the same argument, we could in principle also drop the sweep-back term which is apparently negligible for $r_{1,2} \ll R_L$. However, we will carry it along for the sake of completeness.

4. Data analysis

Except for the observations at 2.25 GHz and 8.5 GHz, our measurements were not made simultaneously at different frequencies. For this reason, we have to apply timing models to the data in order to keep track of the pulse phase between the observations. A time delay given by Eq. (11) will then appear as a deviation of the observed arrival time from the expected one, determined by the timing model.

4.1. Timing models

Regular timing observations of long period pulsars are made by the Jodrell Bank pulsar group, using the 76m-Lovell telescope (Martin & Lyne in prep.). We consider the timing models obtained from these observations as the best available and use the Jodrell Bank models for the reduction of our data. However, the timing data of many pulsars exhibit deviations from the simple spin-down model including only parameters for the period and period derivative, i.e.

$$\Phi(T-T_0) = \Phi_0 + \nu_P(T-T_0) + \frac{1}{2}\dot{\nu}_P(T-T_0)^2 \quad (13)$$

where $\Phi(T)$ is the rotational phase at time T (measured in the pulsar frame), Φ_0 the phase at T_0, $\nu_P = 1/P$ the pulsar spin frequency and $\dot{\nu}_P$ its first derivative. These rotational variations known as *timing noise* can arise from different kind of processes like discrete jumps in Φ or its derivatives, a systematic value of $\ddot{\nu}_P$ related to a real physical process, "random walks" in one of the spin parameters or even orbital motions (see e.g. Cordes & Downs 1985, hereafter CD85).

From an analysis of many pulsars, it has been shown that the amplitude of the timing noise is strongly correlated with the period derivative, $\dot{P}$, (e.g. CD85, Arzoumanian et al. 1994). Depending on the time interval analyzed, timing residuals may appear as regular variations with fairly large amplitudes (for an impressive collection see CD85). In general one can try to account for such large variations if the second derivative of the spin frequency, $\ddot{\nu}_P$, is included in the spin down model (Eq. 13). Although the resulting value, noticeable by a non-zero $\ddot{P}$, might not have any physical meaning (i.e. it might not be related to a *systematic* physical process), it is desirable to do so if one tries to phase align pulse profiles observed at widely spaced epochs. Although the Jodrell timing models include such fits

Table 1. Summary of observations. Besides the observing frequency and the epoch of observation, we quote the used bandwidth, the typical system temperature, T_{sys}, the gain of the telescope, G, and the type of the analyzed signals. Total power signals were obtained by adding gain-corrected LHC and RHC signals.

ν [MHz]	Epoch	BW [MHz]	T_{sys} [K]	G [K/Jy]	signal
1410–1710	various	40	25	1.50	total power
2250	14/15-July-94	40/80/200	80	0.5	RHC
	24/25-July-94				
4750	22/23-July-94	500	60	1.45	total power
8500	14/15-July-94	500	50	1.30	total power
	24/25-July-94				
10550	13/14-July-94	300	50	1.10	total power
	24-July-95				
32000	2/3/4-July-94	2000	120	0.37	total power

for the second period derivative, we took nevertheless care that our analyzed observations were done within a short time interval. However, depending on the known timing noise activity (cf. CD85 and discussion below), for some pulsars we will include data observed at different epochs if necessary.

4.2. TOA measurements

The topocentric TOA of a pulse profile was determined by cross-correlating the profile with a high signal-to-noise ratio (S/N) *template*. In order to calculate the maximum of the cross-correlation function (CCF), we applied a least-square fit of a polynomial to the CCF around its maximal peak (Press et al. 1986). The location of the maximum and its corresponding uncertainty, combined with the recorded "time tag" which corresponds to the midpoint of the integration, yielded finally the TOA and its formal error (e.g. Ryba 1991). The actual value of the TOA is affected by the choice of a pulse longitude that is identified with pulse phase zero, i.e. by the choice of a *fiducial point*. Since we want to time profiles measured at different frequencies, it is in general critical that the fiducial point marks the location of the *fiducial plane*. The fiducial plane is the one which contains simultaneously the rotation and magnetic axis of the pulsar as well as the line-of-sight towards the observer. A TOA of a pulse emitted at this longitude will only suffer the delay given by Eq. (11). The choice of any other longitude, on the other hand, would introduce a frequency dependent offset due to a combined effect of a RFM and spreading of the magnetic field lines.

Craft (1970) showed that the midpoint of pulse profiles is such a fiducial point. Phillips & Wolszczan (1992, hereafter PW92) and P92, respectively, investigated dispersion measures and emission altitudes of data observed between 26 MHz and 4.80 GHz. As a selection criterion, PW92 restricted their sample of pulsars to those with simple or double component profiles, so that a determination of the profile midpoint was possible with high accuracy. Our sample, however, is determined by other aspects, i.e. the ability to detect the sources at the highest possible frequencies. Therefore, our sources do generally not exhibit such regular pulse shapes as would be desirable for a straightforward choice of the fiducial point. Consequently, we used a special technique reported by Kramer et al. (1994) in order to determine the profile midpoint. We first separated the profile into individual components by fitting Gaussians curves to the pulse shape. Averaging the results of several such fits applied to different data, we obtained the mean properties of individual components. These mean components were finally combined again to form a typical average waveform. Since this average waveform represents the sum of several pure Gaussians curves, it is completely free of noise and, therefore, the ideal template for timing.

This approach has three major advantages. Besides the fact that the obtained profile template has an infinitely large signal-to-noise ratio, S/N, the determination of the profile midpoint, even in cases of rather complicated pulse shapes, is fairly accurate since the template is a composition of well defined functions. For the same reason, the template is also independent of any profile resolution since it can be scaled to match any possible gridding of the real data. This ensures, that regardless of the actual resolution chosen during the observations, the same template with the same determined fiducial point can always be used for the analysis.

For observations made at 1.41 GHz, 4.75 GHz and 10.55 GHz, respectively, we constructed the template out of fit results presented by Kramer (1994), since they reflect the results of a large number of independent measurements. For observations at 2.25 GHz and 8.5 GHz, fewer independent measurements were typically available, so that resulting TOAs have larger uncertainties. The 32-GHz profiles were of much lower S/N and of generally simple waveform (cf. Kramer et al. 1996), so that in most of the cases, we thus chose the profile peak as the fiducial point.

4.3. Profile alignment

In order to align pulse profiles, corresponding topocentric TOAs were converted into arrival times at the solar system barycentre using Jodrell Bank timing ephemeredes (Martin & Lyne in prep.), the pulsar timing software TEMPO (Taylor & Weisberg 1989) and the DE200 ephemeris of the Jet Propulsion Laboratories (Standish et al. 1992). The resulting barycentric arrival times were finally corrected for dispersion delays by transform-

ing them into arrival times at a formal infinite radio frequency using Eq. (4) and DM-values determined from the Jodrell observations. The resulting TOA residuals, i.e. the phase differences of the observed arrival times to those expected from the timing model, were used to shift the corresponding pulse profiles with respect to each other. From each timing residual we additionally subtracted the phase offset for the profile measured at the lowest frequency, so that the TOA of this profile is identified with phase zero.

In contrast to most analyses of timing data (e.g. Manchester & Taylor 1977), we adjusted only the global phase offset Φ_0 (cf. Eq. 13) to minimize the TOA residuals. Most importantly, we did not adjust the dispersion measure, DM! This is in contrast to all previous, low frequency studies (e.g. PW92), since at low frequencies the dispersion measure is actually *the* crucial parameter. The use of a DM-value which deviates only slightly from the true value can lead to dramatic results which might be even interpreted as new physical phenomena. A few authors (Shitov & Malofeev 1985; Kuzmin 1986; Shitov et al. 1988), for instance, have reported that low frequency data lead to systematic larger dispersion measures than those obtained at high frequencies, referring to it as *superdispersion*. Phillips (1991a) subsequently demonstrated that the origin of this effect was spurious and originated from small errors in the dispersion measure (of the order of one part in 1000) possibly due to a combined effect of DM-variability, fiducial point ambiguities and a certain choice of the actually used value of the dispersion constant, α_D (cf. Sect. 2).

Our approach to keep the DM-value fixed, is justified by the following estimation. PW92 found long term variations of the dispersion measure as large as $\Delta DM = 0.01$ cm^{-3}pc. During our analysis, we mainly tried to align profiles between 2.25 GHz and 32.00 GHz. Therefore, the same ΔDM possibly existing in the used timing model would produce a time offset of only Δt(32.00 GHz – 2.25 GHz)=8.2μs, which is, less than our typical measurement accuracy for long period pulsars of $P/1024$.

Supposing that pulsar ephemeris describes *perfectly* the observed timing behaviour and that the data are unaffected by retardation, aberration or magnetic field sweep-back. An adjustment of only the phase offset then means that the choice of the pulse longitude actually used for the TOA calculation will not affect the proper alignment at all. In fact, if the determined profile midpoint does not coincide with the proper fiducial point, the offset between these two longitudes will be just the resulting timing residual. Since each profile is shifted according to the associated timing residual, the pulse longitude corresponding to the adopted TOA will be obviously shifted into the proper position. This is, of course, only true in case of perfect timing models and absence of additional physical effects. On the other hand, if the effects which we are interested in, are measurable, the profile midpoint should indeed deviate from its expected position at phase zero. Thus, when we look for effects of retardation, aberration or magnetic field sweep-back, we look for deviations of the determined profile midpoint from the expected arrival time. In cases where the chosen fiducial point does obviously not coincide with the profile midpoint (e.g. for B1133+16 at 32 GHz where only the remaining component remains visible), the point marked in the plots (and its deviation from phase zero) does not have a physical meaning.

5. Results

Results of profile alignments are presented in the following sections for all sources detected at mm-wavelengths.

5.1. PSR B0329+54

Some of our data for this pulsar have already been presented by Kramer et al. (1996) to demonstrate its moding activity at mm-wavelengths. In Fig. 1a we show results of those observations which are summarised in Table 1. The location of the chosen fiducial point is marked by the horizontal errorbar beneath each profile. The length of this error bar indicates the effective resolution, which in general also indicates the accuracy of the fiducial point, is the larger of *either* that of the original data (sampling time) *or* that imposed by interstellar dispersion *or* that obtained after smoothing the data (e.g. at mm-wavelengths). A dotted vertical line indicates the pulse longitude identified with pulse phase zero. The data are consistent with simultaneous arrival times at each frequency. A conservative upper limit derived for the total time delay (not taking the uncertainties in the location of the profile midpoint into account) corresponds to the largest TOA residual difference between two single measurements with respect to each other, i.e. 1590 μs. Upper limits determined for the following other sources are derived similarly.

5.2. PSR B0355+54

The upper two profiles shown in Fig. 1a–db were obtained in December 1994. During one of these observations at 32 GHz, we detected this pulsar in its abnormal mode which is fairly rare at high frequencies (cf. Morris et al. 1980 and Xilouris et al. 1995). The occurrence of mode changing apparently affects the location of leading component within the profile. While observations at 32 GHz (normal mode), at 8.5 GHz and at 10.55 GHz were made in July 1994 (see Table 1), the presented 4.75-GHz profile (whose resolution is limited by dispersion smearing) was obtained in December 1994. A pulse profile at 2.25 GHz was not available due to a contamination of the data by RF-interference. All profiles seem to arrive simultaneously. A corresponding upper limit for the total time delay is 300μs.

5.3. PSR B0540+23

In contrast to our normal analysis, we have chosen the profile peak as the fiducial point since the *trailing part* is visible at low frequencies, and undetectable at 32 GHz. This pulsar is already fairly weak at 4.75 GHz and almost not detectable at 32 GHz. The best profile available at mm-wavelengths was obtained in February 1994. In order to align it with lower frequency profiles of reasonable S/N, we added observations of April 1994 (1.410 GHz and 1.615 GHz profiles). Although we applied the timing

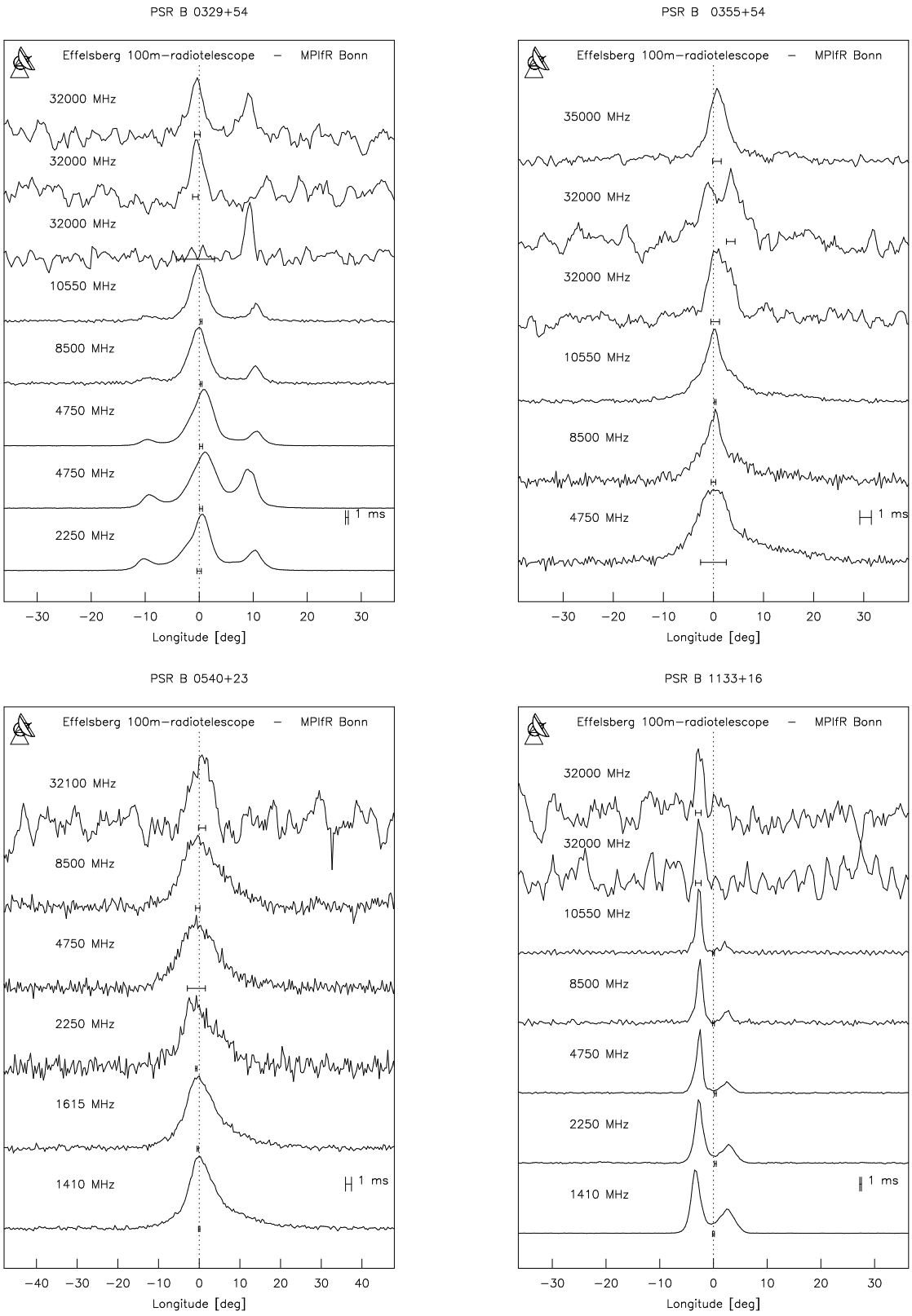

Fig. 1a–d. Time aligned profiles of **a** B0329+54, **b** B0355+54, **c** B0540+23 and **d** B1133+16. The chosen fiducial point is marked by the errorbar beneath each profile, indicating the corresponding resolution (see text). Phase zero is shown as the vertical dotted line and is identified with the TOA of the lowest frequency profile.

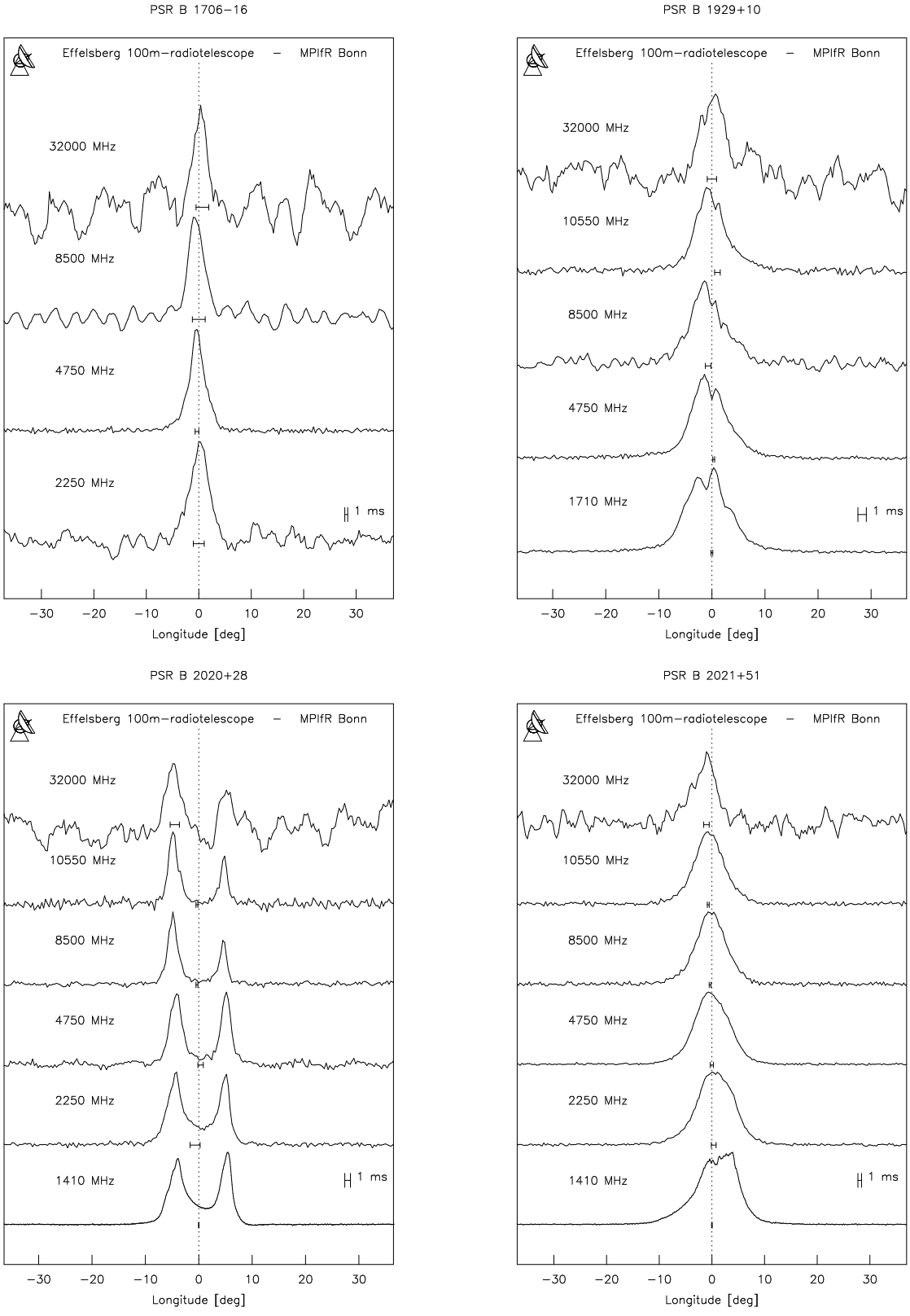

Fig. 2a–d. Time aligned profiles of **a** B1706−16, **b** B1929+10, **c** B2020+28 and **d** B2021+51. See Fig. 1 for details.

model by only adjusting the phase offset, all profiles align perfectly well (Fig. 1c). Despite the low S/N of most of the data, an upper limit for the total time delay of 530 μs is derived.

5.4. PSR B1133+16

Similar to the lower frequency results published by PW92, this pulsar is a "text–book" example for perfect alignment over a large frequency range (Fig. 1d). In order to demonstrate the very little change in profile width and shape already above 1.41 GHz, we added a corresponding 21cm-profile measured in July 1995. Although this latter measurement was done one year after the observations at highest frequency profiles, again an adjustment of only the phase was sufficient (cf. CD85). Obviously, the data are consistent with simultaneous arrivals at all frequencies. As an upper limit for a time delay we find 1640 μs.

5.5. PSR B1706−16

For this pulsar we present pulse profiles at 2.25 GHz, 4.75 GHz, 8.5 GHz and 32 GHz, respectively (Fig. 2a). Data at 8.5 GHz were contaminated by RF-interference and therefore smoothed as the data at 32 GHz. We determine an upper limit for a time delay between different frequencies of 1260 μs.

5.6. PSR B1929+10

Since the 2.25 GHz profile of this pulsar measured in July 1994 was contaminated with radio interference, we represent a 1.71 GHz pulse shape from August 1994 instead (Fig. 2b). An extended emission from the main pulse complicates the exact determination of the profile midpoint. The *chosen* fiducial point of the 10.55-GHz profiles arrives slightly later than expected. However, a careful inspection of the pulse shape suggests that this effect is spurious and due to the complicated waveform which exhibits a slowly declining trailing component. In fact, the first resolvable component brightens with frequency and remains (as far as it can be inferred from the lower S/N) as the only one detected at 32 GHz. At the same time, the strong middle component of the 1.71 GHz profile fades and is completely covered by the first component at high frequencies. However, this development in the pulse shape seems mainly to occur at frequencies below 4.75 GHz. Above this frequency almost no changes, i.e. neither in shape nor pulse width, are observed and all profiles seem to arrive simultaneously. In this case, the upper limit for the time delay is governed by the uncertainty of the location of the fiducial point. We estimate this uncertainty to be about 590 μs.

5.7. PSR B2020+28

This pulsar was reported to exhibit a peculiar timing behaviour at high frequencies (Kuzmin et al. 1986). The data presented by Kuzmin et al. obtained at 102.5 MHz, 4.6 GHz and 10.7 GHz suggested that the pulses observed at 10.7 GHz arrived 5 ms (i.e. the half width of the profile!) *earlier* than it would be expected from a normal dispersion delay. In order to compensate for this delay, a dispersion measure exceeding the usual low frequency value had to be applied to the data to align the profiles properly. As an alternative explanation for this excess in the DM-value, it was argued that magnetic quadrupoles existing in the emission region near the star alter the field structure in a way that high frequency emission is beamed towards earlier times. PW92 reported a similar behaviour for B0525+21 and B1237+25. Again, pulses observed at high frequencies, i.e. 4.8 GHz, seemed to arrive earlier.

In Fig. 2c we now present pulse profiles of B2020+28 obtained in a frequency range between 1.41 GHz (we show a high resolution profile measured in April 1995) and 32 GHz. Adjusting *only* the phase offset, the data align perfectly, although the adopted DM-value was derived at low frequencies. In particular, we do not detect any delay between 4.75 GHz and 10.55 GHz as Kuzmin et al. (1986). Our data are actually consistent with a simultaneous arrival at all frequencies. An upper limit of 1035 μs for the time delay was determined. Possible reasons for the result of Kuzmin et al. (1986) could be the use of insufficiently accurate ephemeris or an error in the clock system during observations. A similar analysis of the other peculiar cases presented by PW92 appears to be difficult, since B0525+21 and B1237+25 are very weak radio sources at high frequencies (Seiradakis et al. 1995).

5.8. PSR B2021+51

A simple inspection of the relative locations of the fiducial markers in Fig. 2d suggests that high frequency profiles arrive slightly earlier than low frequency ones. However, although the profiles look simple in their form, they show a significant profile development which affects the choice of the fiducial points as the profile midpoints. In fact, the profile develops from a double-peaked profile at 0.43 GHz (e.g. Gould 1994) to a simple Gaussian form above 4.75 GHz. Fig. 2d demonstrates that the single component remaining at high frequencies is certainly dominated by the first one of the lower frequency components. The arrival times of the data are then consistent with an upper limit of 1650 μs for a total time delay.

6. Discussion

We noted earlier that at 2.25 GHz we only obtained right-hand circular signals. This can lead to uncertainties in the analysis since the emission of many pulsars exhibits a significant circularly polarised component, so that the location of the *measured* profile midpoint might differ in comparison to a total power profile. Moreover, the propagation time of a signal through the ionized interstellar medium depends also on the sense of the wave polarisation. The difference in arrival times between left-hand and right-hand circularly polarised signals is given by

$$\delta t_{pol} = 0.0572\ \nu_{GHz}^{-3}\ RM \quad \text{[ns]} \tag{14}$$

whereas RM is the *Rotation Measure* of the source in units of rad m^{-2} (e.g. Phillips 1991b). The value of RM is a measure of the Faraday rotation occurring to the pulsar signals along the line-of-sight. Measured values are as large as $\pm$1000 rad m^{-2} (Taylor et al. 1993). However, even for such large RMs the time difference at our lowest frequency, viz. at 1.41 GHz, is only 21

ns and therefore far beyond the accuracy of our measurements. The effect of possible profile changes on the measured TOAs can be estimated by comparing TOA offsets between profiles obtained from LHC and RHC data at 1.41 GHz. For our sample of sources, the amount of circular polarization at 1.41 GHz is less than 15% (Gould 1994), decreasing at higher frequencies (Xilouris et al. 1996). Therefore, TOA offsets determined between LHC and RHC profiles at 1.41 GHz obviously represent safe upper limits for the uncertainty which is introduced if we use RHC signals rather than total power signals at 2.25 GHz. As the result of such an analysis, we find that the TOA-offsets are largest for B0329+54 (i.e. 670 μs) but always smaller than one sampling interval. Our results are therefore not affected by the characteristics of the received signals at 2.25 GHz.

Another effect which could influence the measurements of our TOAs as a function of the emission height, and thus frequency, is that due to curved spacetime near the neutron star. This effect might become important if the emission is (as we will see) created close to the pulsar surface. Gonthier & Harding (1994) examined the importance of such general relativistic corrections and found that, because of spacetime curvature, a photon is observed to have an extra delay in its travel time by as much as 80μs for an emission height directly at the pulsar surface. Depending on the direction in which the photon is emitted this time delay might slightly increase by another 10μs. Even for low emission altitudes the extra time delay is therefore smaller than 90μs and obviously negligible compared to our sampling time and thus our measurement accuracy when observing slowly rotating pulsars. In fact, the largest uncertainties in our results are certainly determined by the general limited S/N at high frequencies. However, the applied technique to determine the profile midpoint and the quality of the timing models meant that we only had to adjust the pulse phase. This ensures sufficient accuracy necessary to draw the following conclusions.

Since the observed change in profile width is generally negligible (see Figs. 1 & 2 and Xilouris et al. 1996), the hollow cone model implies that the emission comes from well inside the light cylinder, i.e. $r_{em} \ll R_L$. Otherwise we would expect significant changes over small frequency intervals. Therefore, we can safely ignore the magnetic field sweep back in the timing analysis. The expected difference in the TOAs of pulse profiles measured at different frequencies is, then, solely determined by the retardation and aberration effect. If the dispersion delay has been removed from the data, we obtain

$$\Delta t_{tot} = \frac{\Delta r_{em}}{c}\,(1+\sin\alpha)\,. \tag{15}$$

Knowing the magnetic inclination, α, we can use the upper limits derived from the data to constrain the size of the emission region, Δr_{em}, i.e.

$$\Delta r_{em} \le \frac{\Delta t_{tot}^{max}\,c}{1+\sin\alpha} \equiv \Delta r_{em}^{max} \tag{16}$$

For many sources, magnetic inclination angles, α, have been determined by various authors (e.g. Lyne & Manchester 1988; Rankin 1990; BCW; Rankin 1993a,b). Depending on the applied technique the obtained values may differ, although in the cases discussed here the published values for α generally agree among various authors. In Table 2 we list those angles α (and their associated reference) which we adopted for our analysis. The resulting maximum size of the emission region for radiation observed at frequencies between 2.25 GHz (or 1.41 GHz, respectively) and 32 GHz are presented in column 5 of the same table. Nevertheless, the true value of α might differ from the one adopted, so that we additionally computed the height of the emission region for the case of an aligned geometry, upper limit (column 6). Apparently, the emission seems to be created within a very compact region and, in fact, our data seem also to be consistent with the assumption that all high frequency emission originates from virtually the same place.

So far, the obtained results constrain only the *size* of the emission region. In contrast, a geometrical method using a comparison between measured pulse widths and geometrical predictions from dipolar models can yield *absolute* emission heights. Such absolute values are, however, model dependent and necessarily underestimated for two reasons. First, for an application of the method we have to assume filled emission beams, i.e. the profile boundaries have to be determined by the last open field lines, which might not hold true for some pulsars (cf. Lyne & Manchester 1988). Second, only the application of a full profile width, viz measured at a very low intensity level (i.e. $< 1-2\,\%$), could yield true values (cf. Gil & Kijak 1993). However, profile widths are generally measured at a 10%-level, thus, leading only to lower limits for emission altitudes (see discussion by Xilouris et al. 1996).

The derived lower limits for the absolute emission heights are nevertheless useful in order to investigate quantitatively the index of a RFM, κ, introduced in Eq. (1). Using lower limits for emission altitudes of 32 GHz radiation, r_{32}^{min}, we can yield an upper limit for κ from the simple relation

$$\kappa \le \log\left(\frac{\Delta r_{em}^{max}}{r_{32}^{min}}+1\right) / \log\left(\frac{\nu_{GHz}}{32}\right) \equiv \kappa^{max} \tag{17}$$

whereas r_{em}^{max} is the maximum time delay between emission at the frequency ν_{GHz} measured in GHz and 32 GHz. Applying emission altitudes, r_{32}^{min}, presented by Xilouris et al. (1996) and also listed in Table 2, we derive upper limits, κ^{max}, quoted in column 9 of Table 2. The actual value of κ probably depends on pulsar dependent parameters like period or period derivative, but if we average the listed values, we can obtain a "mean upper limit" of $<\kappa^{max}>= 0.29 \pm 0.06$. Such value agrees well with the result of BCW ($\kappa = 0.2 \pm 0.1$), PW92 ($\kappa \le 0.66$) and Kijak & Gil 1996 ($\kappa = 0.21 \pm 0.07$). Kramer et al. (1994) and Hoensbroech & Xilouris (1997) investigated in particular the high frequency behaviour of a RFM (i.e. for $\nu > 1$ GHz), and found a typically lower value of $\kappa = 0.11 \pm 0.02$ and $\kappa = 0.15 \pm 0.08$, respectively. Therefore, RFM might be less significant at high frequencies, which is supported by our results (see Figs. 1 & 2) and those of Xilouris et al. (1996), i.e. the pulse shapes and profile widths seem to stop changing above a few GHz, indicat-

Table 2. Origin of high frequency radio emission. We quote the pulse period (column 2) and the magnetic inclination, α (column 3) used for the calculations. The upper limit for the time delay between TOAs measured in a range from 2.25 GHz to 32.00 GHz, Δt_{tot}^{max} (column 4), leads to the maximum size of the corresponding emission region, Δr_{em}^{max}, quoted in column 5 in units of stellar radii, $R_\star \equiv 10$km. Since the actual value of α could be different from the value quoted in column 2, we calculated also the maximum height of the emission region assuming aligned rotators, i.e. α=0 (column 6). Assuming a dipolar magnetic field, Xilouris et al. (1996) derived absolute emission heights from profile widths, r_{32}^{min}, listed in column 7. The size of the emission region derived for frequencies between (generally) 0.1 GHz and 32.0 GHz by Xilouris et al. (1996), Δr_{em}^{geo}, is given in column 8 also in units of $R_\star$. Upper limits for the RFM index κ obtained from Eq. (17) are listed in column 9.

PSR B	P (s)	α ($^\circ$)	Δt_{tot}^{max} (μs)	Δr_{em}^{max} ($R_\star$)	Δr_{em}^{max} (α=0) ($R_\star$)	r_{32}^{min} ($R_\star$)	Δr_{em}^{geo} ($R_\star$)	κ^{max}
0329+54	0.715	30.8[a]	1590	32	48	32±20	55	0.28
0355+54	0.156	51.0[b]	300	5[††]	9	12±3	50	0.18
0540+23	0.246	163.0[c]	530	12[†]	16	4.2±0.5	10	0.44
1133+16	1.188	147.0[c]	1640	31[†]	49	–	15[*]	–
1706−16	0.653	55.3[a]	1260	21	38	12.1±0.9	20	0.37
1929+10	0.227	35.0[d]	590	11[‡]	18	60.3±0.4	30	0.06
2020+28	0.343	71.2[a]	1035	16[†]	31	18±7	25	0.21
2021+51	0.529	23.0[b]	1650	36	50	13.0±0.4	20	0.49

[a] Lyne & Manchester (1988), [b] Rankin (1993a), [c] Blaskiewicz et al. (1991) [d] Phillips (1990)
[††] valid in a frequency range from 4.75 GHz up to 32.00 GHz
[†] valid in a frequency range from 1.41 GHz up to 32.00 GHz
[‡] valid in a frequency range from 1.71 GHz up to 32.00 GHz
[*] valid in a frequency range up to 10.55 GHz

ing that the emission originates from the same magnetospheric region.

It is of interest to investigate how our derived upper limits for κ compare with theoretical models. Certainly, our upper limit for κ is at variance with the classical Ruderman & Sutherland (1975) model, which predicts a value of κ = 0.66. In the theory of Beskin et al. (1988, 1993), κ is expected to be 0.33 which seems to be only just consistent with our upper limit. Luo (1993) expects a similar value of κ = 0.36. In all these models it is, however, assumed that the Lorentz factors of the emitting particles are frequency independent. Any frequency dependence of the Lorentz factors would affect the scaling. Barnard & Arons (1986) suggest that all radiation is created in a narrow range of radius, and that actually refraction effects in the pulsar magnetosphere broadens low frequency pulses, i.e. they basically propose $\kappa \approx 0$. Although this model is therefore consistent with the results shown here, it may have some problems to explain the observed high frequency polarisation properties of some pulsars, e.g. of B1929+10 (cf. Xilouris et al. 1996).

We emphasize that a comparison of the observed data to predictions of various models is in general difficult or even not possible. This is because most of the models are derived to explain only *low* frequency data and, thus, try to account for a relation similar to Eq. (1), i.e. $r_{em}(\nu) = a \cdot \nu^{-\kappa}$. However, including data obtained at the highest radio frequencies, the observations can be apparently better described by a relation like

$$r_{em}(\nu) = a \cdot \nu^{-\kappa} + r_0 \qquad (18)$$

where a constant offset is present (see also Thorsett 1991). Such a relation fits the observations of Xilouris et al. (1996) very well, suggesting that after a well behaving RFM at low frequencies, the emission altitude saturates above a few GHz to a constant value r_0 close to the surface. This lower limit, r_0, can be then identified with the emission altitude derived for 32 GHz emission, r_{32}^{min}, listed in Table 2. A fit of Eq. (1) to data which seem to be better described by Eq. (18) will necessarily lead to inconsistent results.

The result that the emission seems to originate from a small magnetospheric region is, however, unaffected by the actual scaling law. In fact, all major methods applied to derive the size of emission region, i.e. the geometrical method, timing analysis or the polarimetric method introduced by BCW, yield similar results. Emission altitudes derived by BCW using both the polarimetric and geometrical approach for radiation between 0.43 GHz and 1.40 GHz are found within $200R_\star$ from the star, while in most cases the upper bound is only 10–$30R_\star$. Phillips (1992) analyzed timing and pulse width data between 47 MHz and 4.80 GHz. He found that the emission of that frequency range originates within a region of $20R_\star$ in height. Moreover, for PSR B1133+16 in particular, Phillips locates the 4.80 GHz emission in a distance of less than $14R_\star$ from the star, while Cordes (1978) finds for the 1.40 GHz emission of B1133+16 an altitude of less than $63R_\star$. BCW studied, in addition to B1133+16, two other pulsars of our sample, B0540+23 and B1929+10. Their results are also consistent with our emission altitudes (Table 1) since they determine $r_{em} < 85R_\star$ for B0540+23, $r_{em} < 60R_\star$ for B1133+16 and $r_{em} < 57R_\star$ for B1929+10, respectively, which also agrees well with the results of Hoensbroech & Xilouris (1997).

7. Conclusion

In this paper we have constrained the size of the pulsar emission region using high frequency observations made with the Effelsberg radio telescope. Our results indicate that the radiation is created close the neutron star. Close to the neutron star

surface, the emission characteristics might be affected by the presence of magnetic multipoles, resulting in possible deviations of the polarisation angle swing curve from the expected rotating vector model (Radhakrishnan & Cooke 1969), peculiar profile developments or unexplainable timing results. We note that recent results indeed indicate a deviation from a purely dipolar magnetic field in the emission region of *millisecond* pulsars (e.g. Xilouris & Kramer 1996 or Navarro 1996, but see also Gil 1996), which has been previously expected by various authors (e.g. Ruderman 1991). Our presented data on long period pulsars, however, prove that such phenomena are certainly not observed at these high frequencies. This is in contrast to, for instance, the results of Davies et al. (1984) or Kuzmin et al. (1986). In particular, our observations of B2020+28, where an analysis has only included a fit of the pulse phase, suggest that previous results were probably influenced by instrumental effects. We therefore conclude that higher order magnetic multipoles are *not* existing in the emission region of *long period* pulsars.

Acknowledgements. We thank an anonymous referee for pointing our attention to the possible impact of general relativity on our results. This work was in part supported by the European Commission under the HCM Network Contract Nr. ERB CHRX CT960633, i.e. the *European Pulsar Network*. KMX acknowledges the support of an Alexander-von-Humboldt fellowship. Arecibo Observatory is operated by Cornell University under cooperative agreement with NSF.

References

Arzoumanian Z., Nice D.J., Taylor J.H., Thorsett S.E., 1994, ApJ, 422, 671
Barnard J.J., Arons J., 1986, ApJ, 302, 138
Beskin V.S., Gurevich A.V., Istomin Ya.N., 1988, Astroph. Space Sci., 146, 205
Beskin V.S., Gurevich A.V., Istomin Ya.N., 1993, *Physics of the Pulsar Magnetosphere*, Cambridge University Press, Cambridge
Blaskiewicz M., Cordes J.M., Wasserman I., 1991, ApJ, 370, 643 (BCW)
Cordes J.M., 1978, ApJ, 222, 1006
Cordes J.M., Downs G.S., 1985, ApJS, 59, 343 (CD85)
Craft H.D., 1970, Ph.D. thesis, Cornell University, Ithaca, New York
Davies J.G., Lyne A.G., Smith F.G., et al., 1984, MNRAS, 211, 57
Gil J.A., 1996, to appear in *Proc. of IAU Colloq. #160, Sydney*, eds. Johnston, S., Walker, M., Bailes M., PASP
Gil J.A., Kijak J., 1993, A&A, 273, 563
Gold T., 1968, Nature, 218, 731
Gonthier P.L., Harding A.K., 1994, ApJ, 425, 767
Gould D.M., 1994, PhD-thesis, University of Manchester
Hoensbroech A.v., Xilouris K.M., 1997, A&A, in press
Kijak J., Gil J.A., 1996, to appear in *Proc. of IAU Colloq. #160, Sydney*, eds. Johnston S., Walker M., Bailes M., PASP
Kramer M., 1994, A&ASS, 107, 527
Kramer M., 1995, PhD-thesis, University of Bonn
Kramer M., Wielebinski R., Jessner A., et al., 1994, A&ASS, 107, 515
Kramer M., Xilouris K.M., Jessner A., et al., 1996, A&A, 306, 867
Kuzmin A.D., 1986, Sov. Astron. Lett., 12, 325
Kuzmin A.D, Malofeev V.M., Izvekova, V., et al., 1986, A&A, 161, 183
Luo Q., 1993, Ph.D. thesis, University of Sydney
Lyne A.G., Manchester R.N., 1988, MNRAS, 234, 477
Lyne A.G., Smith F.G., 1990, *Pulsar Astronomy*, Cambridge University Press
Manchester R.N., Taylor J.H., 1977, *Pulsars*, Freeman, San Francisco
Martin C.E., Lyne A.G., MNRAS, in prep.
Matese J.J., Whitmire D.P., 1980, ApJ, 235, 587
Morris D., Sieber W., Ferguson D.C., Bartel N., 1980, A&A, 84, 260
Navarro J., 1996, to appear in *Proc. of IAU Colloq. #160, Sydney*, eds. Johnston S., Walker M., Bailes M., PASP
Phillips J.A., 1991a, ApJ, 373, L63
Phillips J.A., 1991b, Ph.D. thesis, Cornell University, Ithaca, New York
Phillips J.A., 1992, ApJ, 385, 282 (P92)
Phillips J.A., Wolszczan A., 1992, ApJ, 385, 273 (PW92)
Press W.H., Flannery B.P., Teukolsky S.A., Vetterling W.T., 1986, *Numerical Recipes: The Art of Scientific Computing*, Cambridge University Press, Cambridge
Radhakrishnan V., Cooke D.J., 1969, Astrophys. Lett., 3, 225
Rankin J.M., 1990, ApJ, 352, 247
Rankin J.M., 1993a, ApJ, 405, 285
Rankin J.M., 1993b, ApJS, 85,145
Rickett B.J., Cordes J.M., 1981, in Sieber W., Wielebinski R., eds, Pulsars, 13 years of Research on Neutron Stars. D. Reidel: Dordrecht, pp. 133-140
Ruderman M.A., 1991, ApJ, 366, 261
Ruderman M.A., Sutherland P.G., 1975, ApJ, 196, 51
Ryba M.F., 1991, Ph.D. thesis, Princeton University
Seiradakis J.H., Gil J.A., Graham D.A., et al. 1995, A&ASS, 111, 205
Shitov Yu.P., 1983, Sov. Astron., 27, 314
Shitov Yu.P., Malofeev V.M, 1985, Sov. Astron. Lett., 11, 39
Shitov Yu.P., Malofeev V.M, Izvekova V.A., 1988, Sov. Astron. Lett., 14, 181
Sieber W., Reinecke R., Wielebinski R., 1975, A&A, 38, 169
Smith F.G., 1969, Nature, 223, 934
Standish E.M., Newall X.X., Williams J.G., Yeomans D.K., 1992, in *Explanatory Supplement to the Astronomical Almanac*, eds. P.K. Seidelmann, Mill Valley, California: University Science Books, p. 279
Taylor J.H., Weisberg J.M., 1989, ApJ, 345, 434
Taylor J.H., Manchester R., Lyne A., 1993, ApJS, 88, 529
Thorsett S.E., 1991, ApJ, 377, 263
Wielebinski R., Jessner A., Kramer M., Gil J.A., 1993, A&A, 272, L13
Wolszczan A., Bartel N., Sieber W., 1980, A&A, 100, 91
Xilouris K.M., Seiradakis J.H., Gil J.A., Sieber W., Wielebinski R., 1995, A&A, 293, 153
Xilouris K.M., Kramer M., 1996, to appear in *Proc. of IAU Colloq. #160, Sydney*, eds. Johnston S., Walker M., Bailes M., PASP
Xilouris K.M., Kramer M., Jessner A., et al., 1996, A&A, 309, 481

This article was processed by the author using Springer-Verlag LaTeX A&A style file *L-AA* version 3.